Original Article

MOLECULAR METABOLISM

Global IP6K1 deletion enhances temperature modulated energy expenditure which reduces carbohydrate and fat induced weight gain

Qingzhang Zhu [1], Sarbani Ghoshal [1], Richa Tyagi [2], Anutosh Chakraborty [1,*]

ABSTRACT

Objective: IP6 kinases (IP6Ks) regulate cell metabolism and survival. Mice with global (IP6K1-KO) or adipocyte-specific (AdKO) deletion of IP6K1 are protected from diet induced obesity (DIO) at ambient (23 °C) temperature. AdKO mice are lean primarily due to increased AMPK mediated thermogenic energy expenditure (EE). Thus, at thermoneutral (30 °C) temperature, high fat diet (HFD)-fed AdKO mice expend energy and gain body weight, similar to control mice. IP6K1 is ubiquitously expressed; thus, it is critical to determine to what extent the lean phenotype of global IP6K1-KO mice depends on environmental temperature. Furthermore, it is not known whether IP6K1 regulates AMPK mediated EE in cells, which do not express UCP1.

Methods: Q-NMR, GTT, food intake, EE, QRT-PCR, histology, mitochondrial oxygen consumption rate (OCR), fatty acid metabolism assays, and immunoblot studies were conducted in IP6K1-KO and WT mice or cells.

Results: Global IP6K1 deletion mediated enhancement in EE is impaired albeit not abolished at 30 °C. As a result, IP6K1-KO mice are protected from DIO, insulin resistance, and fatty liver even at 30 °C. Like AdKO, IP6K1-KO mice display enhanced adipose tissue browning. However, unlike AdKO mice, thermoneutrality only partly abolishes browning in IP6K1-KO mice. Cold (5 °C) exposure enhances carbohydrate expenditure, whereas 23 °C and 30 °C promote fat oxidation in HFD-KO mice. Furthermore, IP6K1 deletion diminishes cellular fat accumulation via activation of the AMPK signaling pathway.

Conclusions: Global deletion of IP6K1 ameliorates obesity and insulin resistance irrespective of the environmental temperature conditions, which strengthens its validity as an anti-obesity target.

Keywords IP6K; Obesity; Diabetes; Energy expenditure; β-oxidation

1. INTRODUCTION

A gain in body fat occurs when energy intake surpasses its expenditure. Therefore, pathways that modulate intake, absorption, or expenditure of carbohydrate or fat energy are prospective anti-obesity targets. Energy is expended by glycolysis and coupled or uncoupled respiration to generate ATP or heat, primarily in the skeletal muscle or brown adipose tissue (BAT), respectively. Classic brown and brown-like beige or brite adipocytes efficiently utilizes energy by the uncoupling protein 1 (UCP1) mediated thermogenesis [1–6]. Cold exposure enhances sympathetic signaling, which primarily induces UCP1 mediated thermogenesis via stimulation of the β-AR (β-adrenergic receptor) mediated c-AMP/PKA pathway [4,7]. Moreover, various other factors such as bile acids, FGF21, atrial and ventricular natriuretic peptides (ANP and BNP), and thyroid hormone (triiodothyronine; T3) induce browning by stimulating their respective receptors, which subsequently trigger overlapping mechanisms [1,4,8,9]. Upon entering target cells, T3 and T4 (thyroxine) are metabolized by the deiodinases [10]. The enzyme DIO2 (type II deiodinase) enhances local concentration of active T3 via deiodination of the inactive T4 form in the adipose tissue [10]. Activated T3 binds to its nuclear receptor and stimulates the transcriptional program necessary to induce UCP1 mediated thermogenesis [11,12].

UCP1 independent thermogenesis has also been reported [13]. For example, chronic stimulation of β3-AR enhances metabolic rate in UCP1-KO mice by increasing mitochondrial biogenesis and fatty acid oxidation in the white adipose tissue (WAT) [14]. Moreover, FGF21 treatment reduces weight gain and restores energy homeostasis in UCP1-KO mice by increasing the transcriptional co-activator PGC1α (peroxisome proliferator-activated receptor gamma coactivator 1-alpha) expression levels in the inguinal WAT (IWAT) [15,16]. Both UCP1 dependent and independent thermogenesis as well as coupled respiration are enhanced by PGC1α [1,7,8,17]. PGC1α promotes these processes by stimulating several transcription factors and co-

[1]Department of Metabolism and Aging, The Scripps Research Institute, Jupiter, FL, 33458, USA [2]The Solomon H. Snyder Department of Neuroscience, Johns Hopkins University School of Medicine, Baltimore, MD, 21205, USA

*Corresponding author. Fax: +1 561 228 3059. E-mail: achakrab@scripps.edu (A. Chakraborty).

Received September 15, 2016 • Revision received November 15, 2016 • Accepted November 23, 2016 • Available online 28 November 2016

http://dx.doi.org/10.1016/j.molmet.2016.11.010

activators [4,17]. PGC1α expression and activity are regulated by various pathways including the AMP activated protein kinase (AMPK). AMPK is a cellular energy sensor [18], which enhances both coupled and uncoupled respiration mediated EE especially in adipose tissue and skeletal muscle [19–23]. Hence, the AMPK activator AICAR (5-Aminoimidazole-4-carboxamide 1-β-D-ribofuranoside) stimulates EE [24,25]. AMPK stimulates PGC1α activity either by direct phosphorylation [26] or by enhancing sirtuin mediated PGC1α deacetylation [22]. The enzyme acetyl CoA carboxylase (ACC) generates malonyl CoA in the fatty acid biosynthetic pathway [27]. Malonyl CoA inhibits fatty acid (β)-oxidation by reducing carnitine palmitoyltransferase (CPT) mediated mitochondrial fatty acid uptake. AMPK phosphorylates and inhibits ACC, which results in reduced fatty acid biosynthesis and increased β-oxidation [18,20].

In mammals, a family of three IP6 kinases (IP6Ks) primarily convert the inositol pentakisphosphate IP5 [I(1,3,4,5,6)P5] and the inositol hexakisphosphate IP6 [I(1,2,3,4,5,6)P6] (inositol hexakisphosphate) to inositol pyrophoshates 5PP-IP4 and 5PP-IP5 (5-IP7), respectively [28–32]. Moreover, in coordination with the enzyme PPIP5K, IP6Ks synthesize 1,5-IP8 [32–34]. At a lower ATP/ADP ratio, IP6Ks dephosphorylate IP6 to a specific form of IP5 [Ins(2, 3, 4, 5, 6)P5] [35]. IP6 and 5-IP7 bind protein targets to modulate their functions [28–30]. In addition, inositol pyrophosphates pyrophosphorylate proteins [28,29]. IP6Ks also regulate certain functions such as lipolysis, via protein-interaction [36–38]. In rodents, IP6K1 is the major isoform in adipose and other tissues, whereas IP6K3 expression is higher in the skeletal muscle [39]. Mice with IP6K1 deletion (IP6K1-KO) are protected from HFD-induced weight gain and insulin resistance [40]. HFD-fed IP6K1-KO mice (HFD-KOs) maintain insulin sensitivity by sustaining activity of the insulin sensitizing protein kinase Akt [40]. IP6K1 is downregulated in IWAT and RWAT (retroperitoneal) depots following cold exposure [41]. Adipocyte-specific IP6K1-KO (AdKO) mice are protected against HFD-induced weight gain, at ambient (23 °C), but not at thermoneutral (30 °C) temperature, although their insulin sensitivity is preserved at thermoneutrality [41]. IP6K1 reduces adipose tissue browning mediated thermogenesis by inhibiting AMPK activity [41]. 5-IP7 inhibits Akt, whereas IP6 stimulates AMPK's stimulatory phosphorylation by upstream kinases [40,41]. Therefore, conversion of IP6 to 5-IP7 by IP6K1 inhibits both the kinases, which regulates insulin sensitivity and thermogenic EE [40]. Accordingly, the pan IP6K inhibitor TNP [N2-(m-Trifluorobenzyl), N6-(p-nitrobenzyl)purine] [42] reduces body weight and insulin resistance via AMPK and Akt activation in diet induced obese mice [41,43].

Although the lean phenotype of HFD-AdKO mice is abolished at 30 °C [41], TNP partly blocks weight gain at 30 °C [43]. This indicates that global-IP6K1 may regulate energy metabolism more robustly than adipocyte-IP6K1. Moreover, whether global IP6K1 deletion enhances browning or IP6K1 regulates AMPK mediated energy metabolism in cells that do not express UCP1 is not known. Here, we determine effects of global IP6K1 deletion on body weight and EE at various diet and temperature conditions. Moreover, we used an array of biochemical assays in UCP1 deficient cells to determine IP6K1's influences in AMPK mediated metabolic processes.

2. MATERIALS AND METHODS

2.1. Materials

QPCR: TaqMan probes were purchased from Life Technologies (Grand Island, NY). **Antibodies**: UCP1 (cat#U6382): Sigma Aldrich, St. Louis, MO; phospho (S473; cat#4060) and total Akt (cat#2920), phospho (S79; cat#3661) and total ACC (cat#3676), phospho (T172; cat#2535) and total AMPK (cat#5831), phospho-AMPK Substrate (cat#5759), acetylated-Lysine (cat#9814): Cell Signaling Technology, Danvers MA; Adiponectin HMW/LMW (cat#5901): BioVision Milpitas, CA; IP6K1 (cat#GTX103949): GeneTex; PGC1α (for immunoblotting, cat#AB3242): EMD Millipore, Billerica, MA; PGC1α (for immunoprecipitation, cat#sc-13067), DIO2 (sc-98716): Santa Cruz Biotechnology, Dallas, TX. **Radiochemicals**: [9, 10-3H(N)]-oleic acid (cat#-NET289001MC), [9, 10-3H(N)]-palmitic acid (cat#NET043001MC) and [3H] Acetic acid (cat#NET003005MC), PerkinElmer Inc., Boston, MA. Unless otherwise stated, all chemicals were purchased from Sigma Aldrich.

2.2. Animals

Animal care and experimentations were approved by the Scripps Florida, Institutional Animal Care and Use Committee (IACUC). Male IP6K1-KOs and WT littermates were used [44]. Mice are housed in groups of 3–5 in a 12 h light/12 h dark cycles at 23 °C and are fed standard chow, unless otherwise stated. Chow (Harlan Laboratories # 2018SX; 16%, 60% and 24% calories from fat, carbohydrate, and proteins, respectively) fed (2-month old) and high fat-fed (chow fed for 2 months followed by high fat diet as indicated; Bioserve#S3282; 59%, 26% and 15% calories from fat, carbohydrate, and proteins, respectively), were used in the studies [40]. At 30 °C, DIO was generated following a standard protocol [45]. Briefly, mice were placed in a 30 °C room immediately after weaning. After one week of acclimatization, mice were fed a HFD for indicated time period. Weekly body weight was monitored. Body composition and GTT were performed at indicated time periods. EE was measured in thermoneutrally placed mice after 15-weeks of HFD feeding, after which, mice were sacrificed by CO_2 asphyxiation for tissue processing. Rectal temperature was measured at indicated time points using the RET-3 probe in a TH-5 thermometer (Physitemp) [41].

2.3. Food intake

Food intake was monitored in CD (Chow diet)-fed mice under fed, fast, and refed conditions using the BioDAQ instrumentation (Research diet) following previously described procedure [41]. Data represent the average daily intake. For HFD-fed animals, food intake was measured at the onset of HFD-feeding, in ad libitum conditions. Average values are compared by two-tailed Student's t-test to determine significance.

2.4. CLAMS

Mice were individually placed and acclimatized in a Comprehensive Laboratory Monitoring System (CLAMS; Columbus Instruments) at 23 °C for 36 h. Afterwards, VO_2, VCO_2, and spontaneous locomotor activity were measured for the indicated time periods. Cold-induced oxygen consumption was assessed by changing the temperature from 23 °C to 5 °C for 24 h followed by 6 h fasting. For the fasting-refeeding study, mice were fasted overnight at 23 °C, after which, food was reintroduced and EE was measured for 10 h. Respiratory exchange ratio (RER) and energy expenditure (EE) were calculated using the following equations: $RER = VCO_2/VO_2$, EE (kcal/h) = (3.815 + 1.232*RER)*VO_2. Values were normalized by lean body mass [41]. Both raw and average values for VO_2, EE, and RER are presented. Based on mean RER values, the exact percentage of VO_2 consumed for carbohydrate and fat oxidation was determined [46].

2.5. Body composition studies

Total, fat, lean, and fluid mass of chow-fed and high fat-fed WTs and IP6K1-KOs were measured using the Minispec LF-NMR (Brucker Optics) analyzer [41].

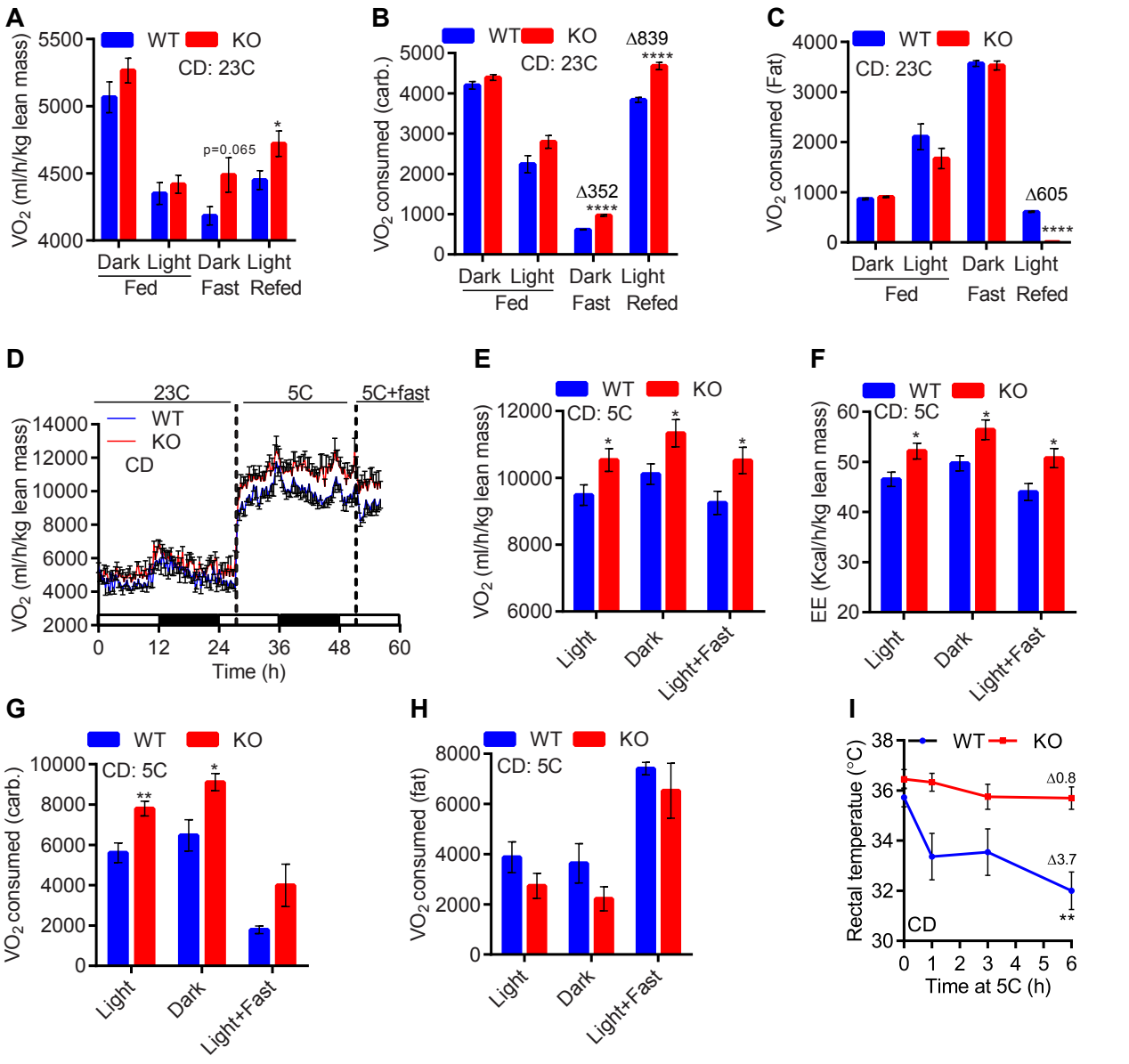

Figure 1: CD-fed IP6K1-KO mice display enhanced carbohydrate oxidation-mediated EE upon fasting/refeeding or following cold exposure. **A**. At 23 °C, CD-fed (ad libitum) WT and IP6K1-KO mice display similar VO_2 consumption. Fasting reduces VO_2 in CD-WTs to a higher extent, than CD-KOs. Refed CD-KO mice also display higher VO_2 consumption ($n = 7–8$ *mice/group; t-test*). **B**. Fasting lowers carbohydrate-VO_2 in both genotypes; yet, the values are higher in the knockouts. CD-KOs also exhibit higher carbohydrate-VO_2 following refeeding ($n = 7–8$ *mice/group; t-test*). **C**. Fat-VO_2 is similar in fed and fasted WT and IP6K1-KO mice. Refeeding lowers Fat-VO_2 in WT mice to a lower extent; thus, CD-KOs oxidize less fat than WT, at this condition ($n = 7–8$ *mice/group; t-test*). **D**. CD-KO mice display similar VO_2 consumption at 23 °C. Acute cold and cold + fast exposed knockouts consume more oxygen than WT ($n = 6$ *mice/group*). **E**. Average VO_2 consumption is enhanced in the CD-KOs following cold and cold + fast exposures ($n = 6$ *mice/group; t-test*). **F**. Average EE is higher in the CD-KOs following cold and cold + fast exposures ($n = 6$ *mice/group; t-test*). **G**. CD-KO mice display higher carbohydrate-VO_2 than WT at 5 °C ($n = 6$ *mice/group; t-test*). **H**. Fat-VO_2 is largely similar in CD-fed WTs and IP6K1-KOs ($n = 6$ *mice/group; t-test*). **I**. Acute cold + fast exposure decreases body temperature in CD-WT whereas IP6K1-KO mice are protected. Mice were kept at 5 °C for 8 h followed by acute (6 h) fasting at 5 °C ($n = 6–8$ *mice/group; two-way Anova*). In all panels, data are expressed as mean ± SEM. *P < 0.05, **P < 0.01, ****P < 0.0001.

2.6. Adipose tissue isolation, histological, and immunohistochemical analyses

Mice were sacrificed, after which, various adipose tissue depots were collected, weighed, and rapidly transferred to liquid nitrogen, followed by storage at −80 °C or in 10% neutral buffered formalin at room temperature until further processing. EWAT (epididymal; embeds the vas deferens and the epididymis), IWAT (inguinal; attached dorsally along the pelvis and skewed ventrally down on to the thigh of the hind limb), RWAT (retroperitoneal; attached on the dorsal wall of the back) and BAT (brown; depots above the shoulder blades) were collected from CD and HFD-fed WT and IP6K1-KO mice were isolated at indicated time periods following a standard procedure [47].

Various adipose tissue depots were sent to Scripps Histology core after appropriate fixation for two days in 10% neutral buffered formalin. Eight micron-sections were prepared and subsequently stained with hematoxylin and eosin (H&E). For UCP1 immunohistochemistry,

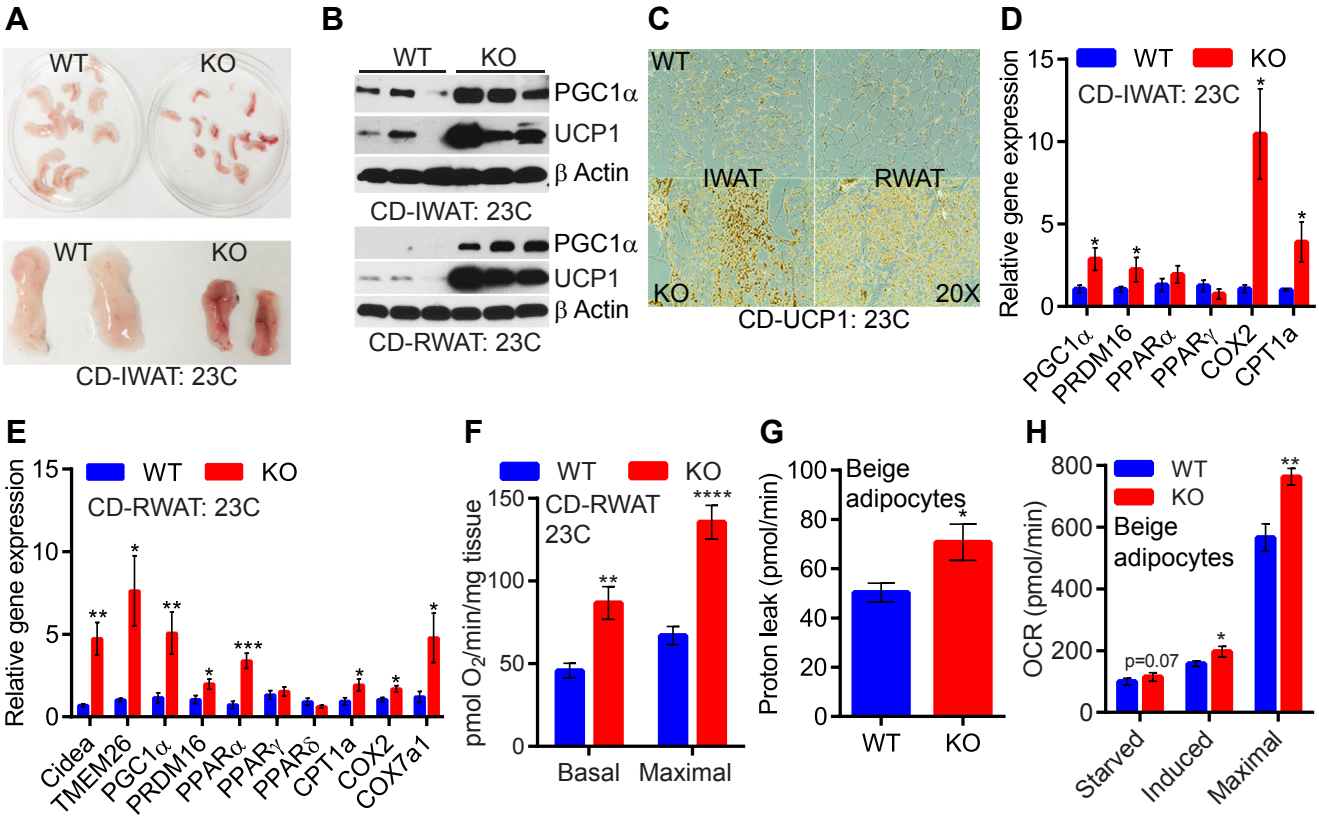

Figure 2: Global IP6K1 deletion stimulates adipose tissue browning. **A**. At 23 °C, CD-KO IWAT appears brownish. **B**. Immunoblot analyses indicate upregulation of UCP1 and PGC1α proteins CD-KO IWAT and RWAT at 23 °C. **C**. Immunohistochemistry of UCP1 also reveals browning in CD-KO IWAT and RWAT at 23 °C. **D and E**. Amplification of the browning and mitochondrial machinery in CD-KO RWAT (*n = 5–7 mice/group, t-test*) and IWAT (*n = 4 mice/group, t-test*) at 23 °C. **F**. RWAT explant isolated from CD-mice at 23 °C displays higher basal and FCCP-induced OCR in the knockouts (*n = 4 mice/group, t-test*). **G**. Proton leak is higher in IWAT-beige adipocytes of CD-KO mice (*n = 6 mice/preparation, 8 replicates, t-test*). **H**. Carbohydrate induced and maximal oxidative capacity are higher in IWAT-beige adipocytes of CD-KO mice (*n = 6 mice/preparation, 8 replicates, t-test*). In all panels, data are expressed as mean ± SEM. *P < 0.05, **P < 0.01, ***P < 0.001, ****P < 0.0001.

primary antibody was detected by Vectastain Elite ABC kit and diaminobenzidine (DAB) reagent using the manufacturer's instructions [41]. Adipocyte size was quantified using ImageJ software.

2.7. Analyses of various plasma parameters

Plasma triglycerides, high-density lipoprotein (HDL), low-density lipoprotein (LDL), and total cholesterol were determined following standard procedures at the TSRI metabolic core facility by using the respective kits (Roche). Plasma T3 was measured using a mouse T3 ELISA kit (cat# IB19128, Immuno-Biological Lab, Inc. IBL-America, MN), following the manufacturer's instructions. Adiponectin complexes were analyzed following standard protocol. Briefly, 1.5 μl of plasma was mixed with Laemmli buffer without β-mercaptoethanol. Proteins were resolved in a 4–15% SDS-PAGE [41,48].

2.8. Glucose (GTT) and AICAR tolerance tests

GTT was measured in thermoneutrally placed HFD-mice following a standard protocol [41]. AICAR was injected following standard procedure. Briefly, 2-month old CD-mice were fasted for 6 h before AICAR (250 mg/kg body weight) injection [49]. Blood glucose, at indicated time points was monitored.

2.9. RNA isolation and real time PCR

RNA isolation and QPCR were performed following standard procedures [41]. CPT1a and PGC1α mRNA in MEFs (mouse embryonic fibroblasts) was assessed 2 h post AICAR (1 mM) treatment. Relative expression was determined using the ΔΔCT method and normalized to the housekeeping gene β Actin.

2.10. Seahorse analyses to determine mitochondrial oxygen consumption rate (OCR)

To determine OCR in the RWAT, XF24 Islet Capture Microplates (#101122) were used [50]. OCR was determined in 3 mg of RWAT tissue in XF assay medium supplemented with 25 mM glucose and 1 mM pyruvate. FCCP (20 μM) was injected to obtain the maximal OCR. Results are presented as pmole/min/mg tissue. Mitochondrial respiration was determined in 3T3-L1 preadipocytes and primary inguinal beige adipocytes following a standard procedure [41]. Beige adipocytes were differentiated from stromal vascular cells isolated from 6 to 8 weeks old mice [41].

2.11. Lipid accumulation in MEFs

WT and IP6K1-KO MEF cells [44] and IP6K1-complemented cells (complemented with vector, catalytically active, and inactive IP6K1) in an IP6K1-KO background were used [40]. Cells were seeded at a density of 1×10^5 cells/well in a 24-well plate. After 24 h, cells were treated with oleate/BSA mixture (0.4 mM; molar ratio = 6:1) for 24 h [51,52]. Lipid was stained with 'Oil Red O' for 2 h and pictures were taken using an EVOS microscope. Afterwards, lipids were dissolved by 100% isopropanol and quantified.

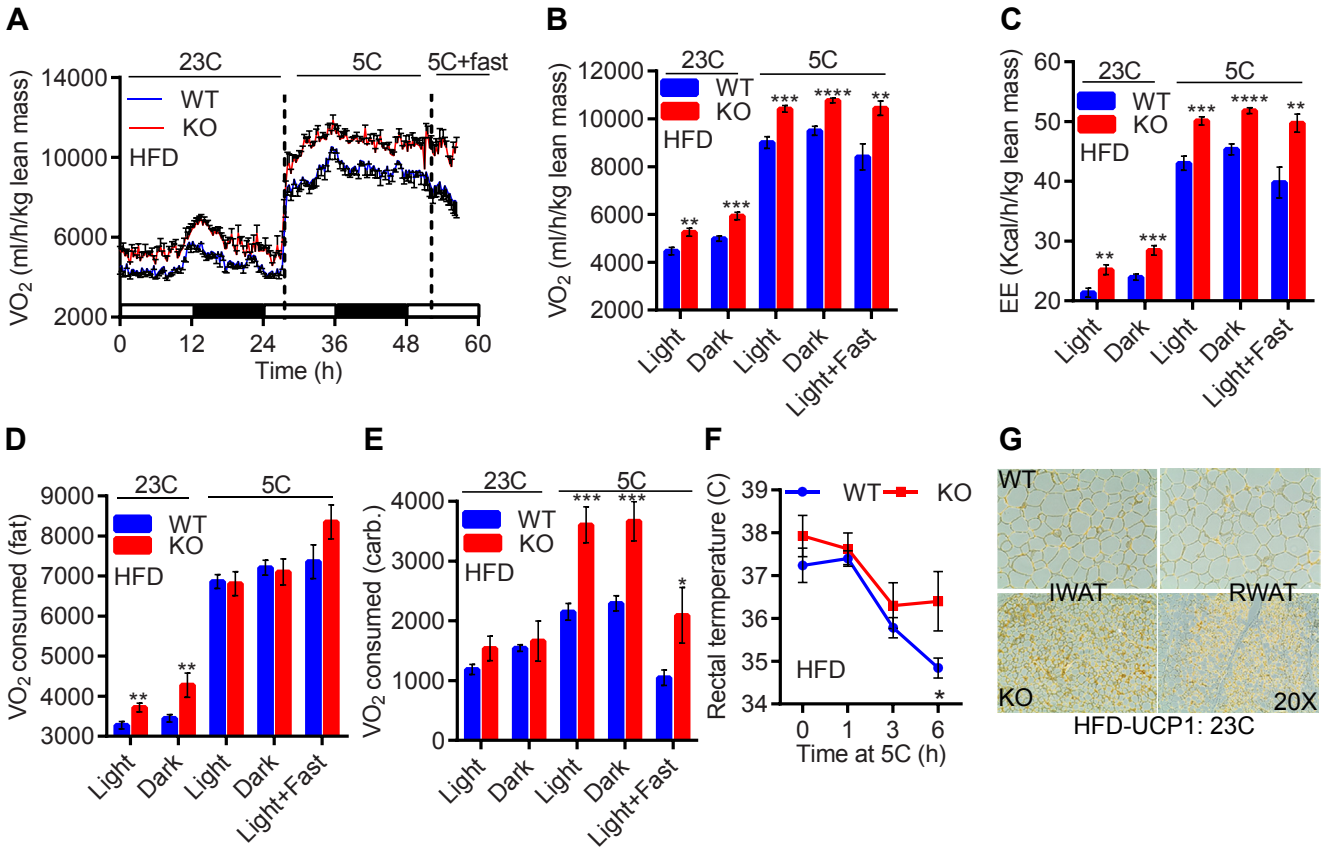

Figure 3: HFD-fed IP6K1-KO mice exhibit higher fat oxidation at 23°C, albeit switch to carbohydrate oxidation at 5°C. **A**. HFD-KOs consume more oxygen than WT, both at 23 °C and 5 °C (*n = 6–9 mice/group*). **B and C**. Average VO_2 and EE are enhanced in HFD-KOs under both temperature conditions (*n = 6–9 mice/group; t-test*). **D and E**. At 23 °C, HFD-KO mice oxidize more fat. However, cold exposed HFD-KOs switch to carbohydrate oxidation (*n = 6–9 mice/group; t-test*). **F**. Cold exposure decreases body temperature in HFD-WT whereas the knockouts are protected (*n = 4–5 mice/group; two-way Anova*). **G**. Immunohistochemistry reveals higher UCP1 protein levels in RWAT and IWAT of HFD-KOs. In all panels, data are expressed as mean ± SEM. *P < 0.05, **P < 0.01, ***P < 0.001, ****P < 0.0001.

2.12. Fatty acid (β)-oxidation and biosynthesis assays

β-oxidation was measured by the production of [3H] H_2O form [3H] OA or [3H] PA under the following conditions; i) basal: treated 2 h with radiolabeled fatty acids; ii) fatty acid induced: treated 24 h with cold fatty acids followed by 2 h treatment of radiolabeled fatty acids and; iii) AICAR or SIRT modulators induced: cells treated with cold fatty acids (24 h) [52] then treated with radiolabeled fatty acids for 2 h in presence of the compounds. β-oxidation was measured following a standard procedure [53]. This assay specifically measures [3H] H_2O, generated by the β-oxidation process [54]. After four steps of β-oxidation, 75% of [3H] from 9,10-[3H] fatty acids generate [3H] H_2O, whereas 25% make [3H] acetyl CoA, of which [3H] H_2O is measured [54]. Fatty acid biosynthesis assay was performed in 8-day differentiated 3T3L1 adipocytes by assessing radiolabeling of fatty acids following [3H] Acetic acid treatment [55].

2.13. Immunoblot and immunoprecipitation studies

Tissues or cells were lysed and processed for immunoblot analyses following standard procedure [41]. Immunoprecipitation of PGC1α from MEFs was performed following standard protocol (Cell Signaling Technology).

2.14. Statistics

Number of mice (n) used in experiments are indicated in each plot. Plots represent quantification results of at least three independent samples/experiments. Immunoblots were quantified using 'ImageJ' software. For multiple comparisons, one-way or two-way Anova with Holm-Sidak multiple comparison tests was used. For two independent data sets, two tailed Student's *t-test* was used. Data are presented as ±SEM (****P ≤ 0.0001, ***P ≤ 0.001, **P ≤ 0.01 and *P ≤ 0.05). Statistical significance was calculated in GraphPad Prism, version 6.

3. RESULTS

3.1. CD-fed IP6K1-KO mice display enhanced carbohydrate oxidation mediated EE upon fasting/refeeding or following cold exposure

At 23 °C, chow (CD)-fed WTs and IP6K1-KOs (CD-KOs) consume [44] and expend similar energy [40], yet the knockouts display slightly less body mass due to reduced fat accumulation [40]. This indicates that transient alterations in diet and/or environmental temperature may enhance EE, which reduces fat mass in the CD-KOs. Therefore, at first, we examined effects of fasting and refeeding on EE in WTs and IP6K1-KOs. CD-fed WTs and IP6K1-KOs consume similar VO_2 at 23 °C (Figure 1A; dark, light). Expectedly, fasting reduced VO_2 consumption in both genotypes, although to a slightly lower extent in the knockouts. Thus, fasted CD-KOs consumed slightly (not significantly) higher oxygen, compared to WT (Figure 1A; fast). Conversely, refeeding increased VO_2 consumption in both genotypes; yet, CD-KOs consumed marginal albeit significantly higher VO_2 (Figure 1A; refed). As

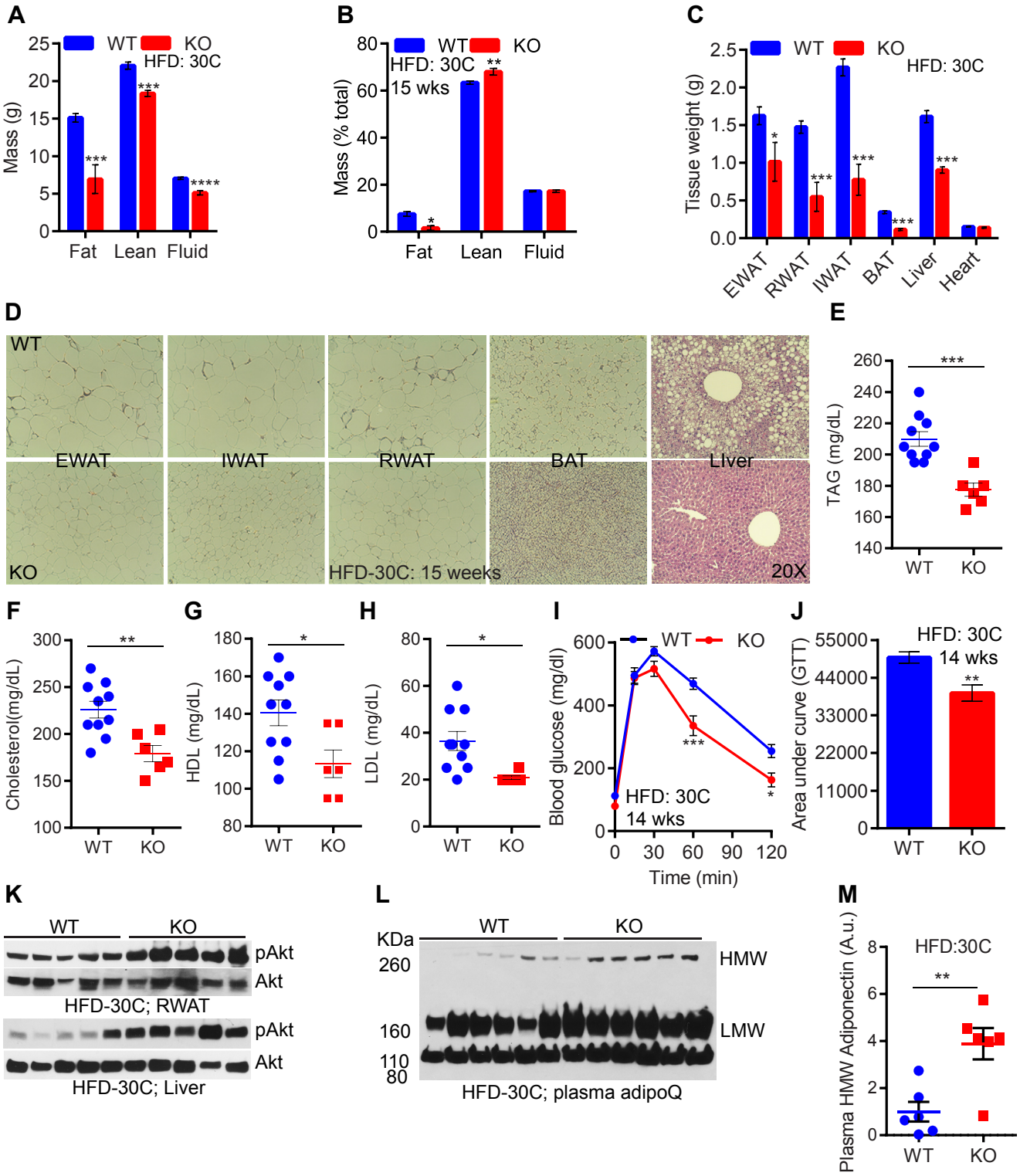

Figure 4: Thermoneutrality delays, yet does not abolish the lean phenotype of HFD-fed IP6K1-KO mice. **A**. After 15-weeks at 30 °C, HFD-fed IP6K1-KO mice display a reduction in total fat, lean, and fluid masses ($n = 6–10$ *mice/group, t-test*). **B**. At this condition, percent (over total body weight) fat is reduced in HFD-KO, whereas percent lean mass is slightly increased. Percent fluid mass is similar in both genotypes ($n = 6–10$ *mice/group; t-test*).**C**. After 15-weeks at 30 °C, HFD-KOs display substantially less weight of various adipose tissue depots and liver but not heart. ($n = 6–10$ *mice/group; t-test*). **D**. HFD-KO mice accumulate less fat in adipocytes of diverse adipose tissue depots. The knockouts are also protected from fatty liver. **E**–**H**. Serum cholesterol, TAG, HDL, and LDL levels are lower in HFD-KOs after 15-weeks at 30 °C ($n = 6–10$ *mice/group; t-test*). **I**. Glucose tolerance test (GTT) indicates that 14-weeks HFD-KOs dispose of glucose more efficiently than WT ($n = 6–10$ *mice/group; two-way Anova*). **J**. Area under curve (AUC) values indicate that glucose disposal is significantly improved in HFD-KOs after 14-weeks of HFD at 30 °C. **K**. Akt stimulatory phosphorylation (S473) is higher in the RWAT and liver of HFD-KOs after 15-weeks at 30 °C. **L and M**. Serum levels of HMW and LMW AdipoQ are higher in HFD-KOs under the same condition ($n = 6$ *mice/group; t-test*). In all panels, data are expressed as mean ± SEM. *P < 0.05, **P < 0.01, ***P < 0.001, ****P < 0.0001.

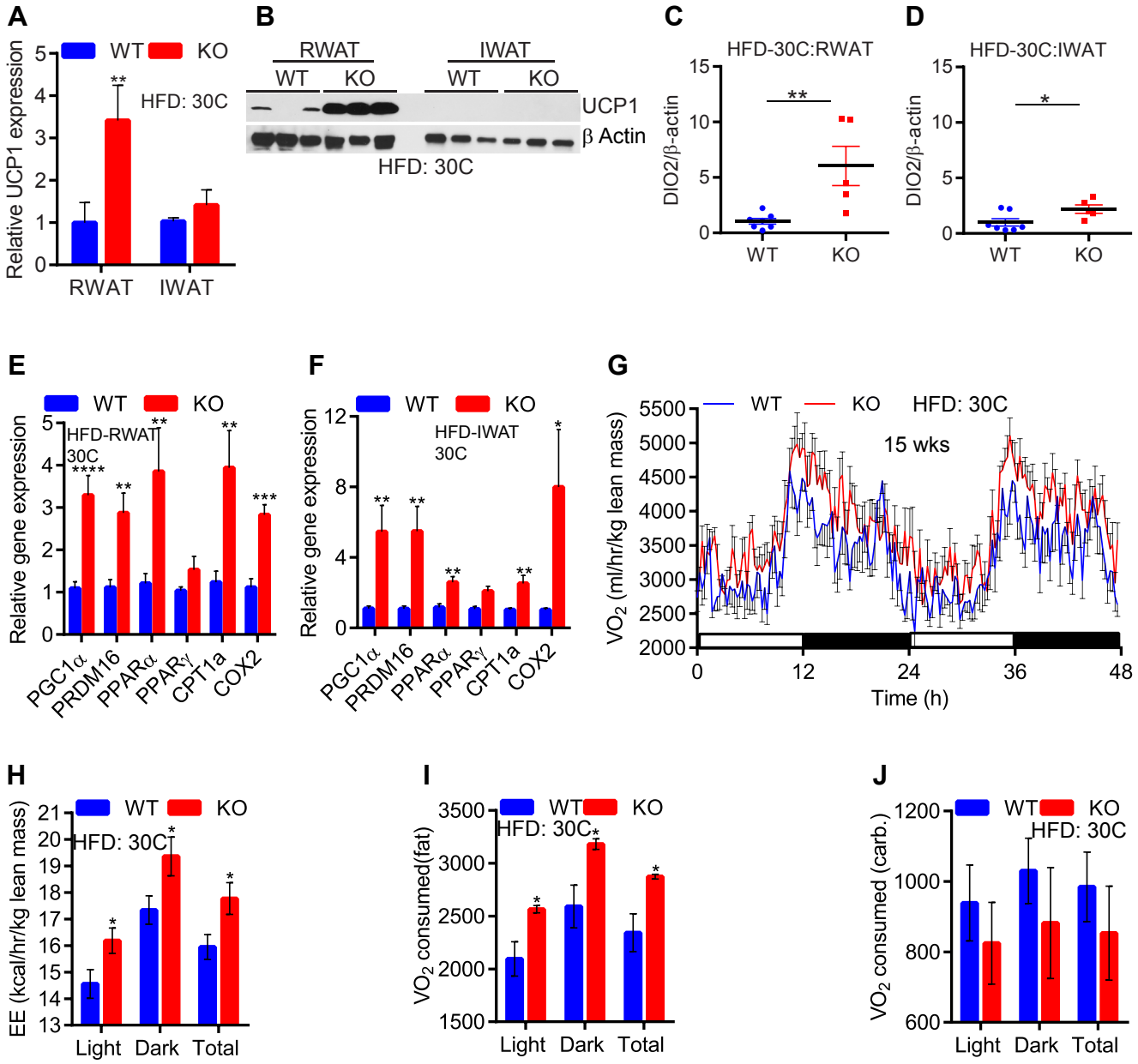

Figure 5: HFD-fed IP6K1-KO mice display greater fat oxidation mediated EE at 30°C. **A**. After 15-weeks at 30 °C, UCP1 mRNA expression is downregulated in the IWAT of HFD-KOs. However, HFD-KO RWAT still display higher UCP1 expression (*n = 6–10 mice/group; t-test*). **B**. UCP1 protein level is higher in HFD-KO RWAT at 30 °C. UCP1 is undetectable in the IWAT under this condition. **C and D**. ImageJ analyses reveal that DIO2 protein level is substantially higher in the RWAT depot of IP6K1-KO mice, whereas its level in the KO-IWAT was also high but to a lesser extent (*n = 5–7 mice/group; t-test*). **E and F**. Mitochondrial EE markers are upregulated in HFD-KO IWAT and RWAT at 30 °C (*n = 6–10 mice/group; t-test*). **G**. After 15-weeks at 30 °C, HFD-KOs display increased VO_2 consumption (*n = 6 mice/group*). **H**. EE is also higher in thermoneutrally placed HFD-KOs (*n = 6 mice/group; t-test*). **I**. At 30 °C, HFD-KOs expend more energy by fat oxidation (*n = 6 mice/group; t-test*). **J**. Carbohydrate oxidation is similar in HFD-WT and IP6K1-KOs at 30 °C (*n = 6 mice/group; t-test*). In all panels, data are expressed as mean ± SEM. *P < 0.05, **P < 0.01, ***P < 0.001, ****P < 0.0001.

previously reported, respiratory ratio (RER) was largely similar in CD-fed and fasted WT and IP6K1-KO mice, although refed knockouts displayed a marginal increase in the RER value (Figure S1A). RER values provide a relative understanding of carbohydrate and fat mediated oxygen consumption among cohorts. However, they do not give the exact amount of oxygen consumed for carbohydrate and fat. Therefore, we calculated these values based on RER and VO_2, in accordance with the literature [46], which revealed that although RER values were not significantly changed (Figure S1A), VO_2 consumed for carbohydrate, but not fat, oxidation was significantly higher in fasted IP6K1-KOs compared to WT (Figure 1B and C; dark + fast). Conversely, refeeding enhanced carbohydrate-VO_2 in both genotypes, yet the average value was significantly higher in CD-KOs (Figure 1B; refed). In contrast, fat-VO_2 is similar in WTs and IP6K1-KOs under fed and fasted conditions (Figure 1C; fed and fast). Refeeding reduces fat-VO_2, to a higher extent in the knockouts (Figure 1C; refed). These results reveal that CD-fed IP6K1-KO mice consume more oxygen for carbohydrate oxidation, whereas their fat-oxidation is less than WT. Nevertheless, the resultant energy expenditure is higher in CD-KOs under fasted and refed conditions, which leads to less fat accumulation. Activity profiles are unchanged (Figure S1B). As observed previously, food intake is not significantly altered in fed CD-KOs (Table S1;

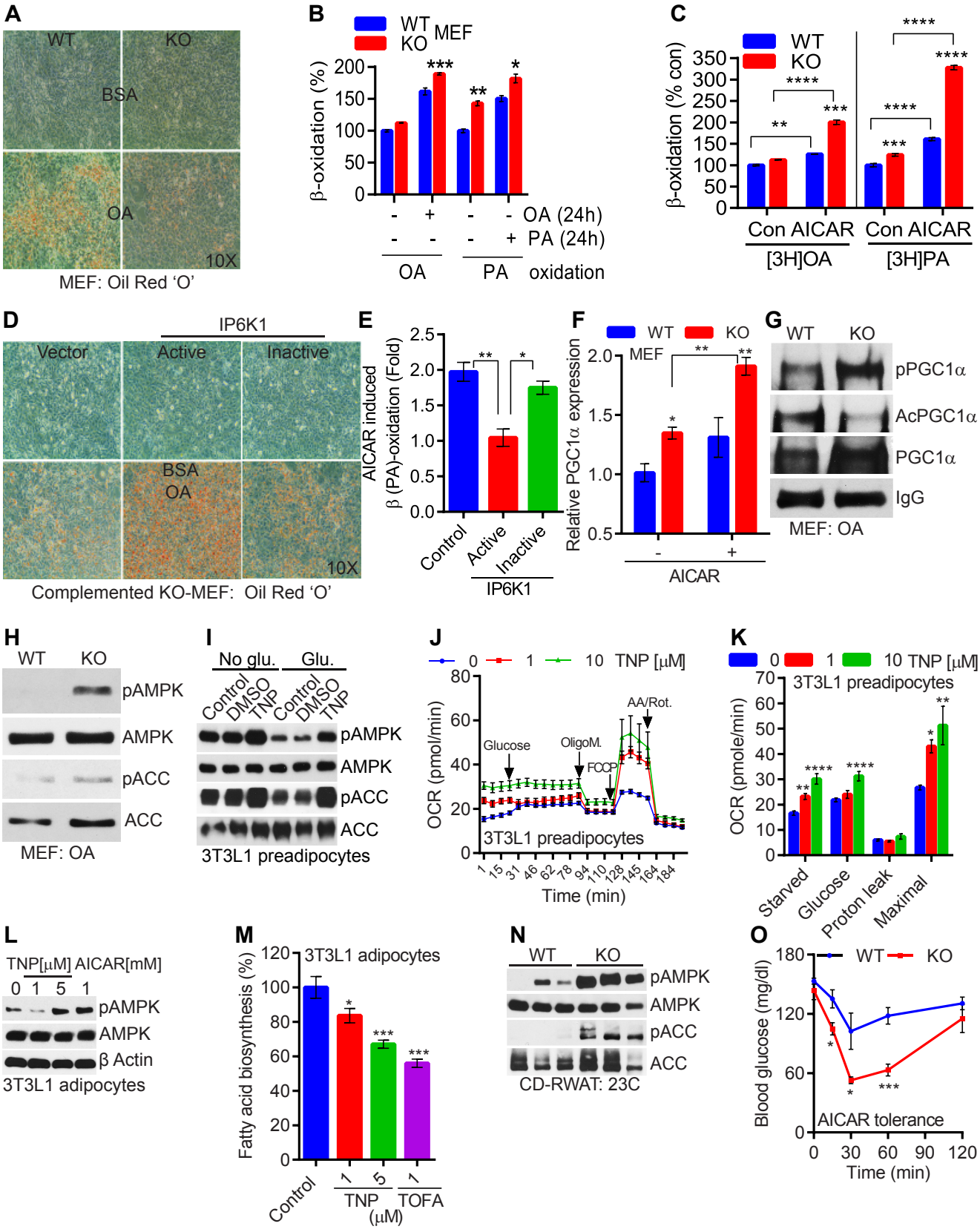

daily intake). However, refeeding increases food intake in the knockouts for a short period of time (4 h) (Table S1; refed), after which it is similar in both genotypes (data not shown). The transient increase in food intake during refeeding in the knockouts, partly compensates for the expended energy during fasting. However, the compensation is clearly not enough, as energy expenditure is also higher in refed-KOs, which leads to less energy accumulation.

Next, we monitored whether environmental temperature variations differentially influence EE in CD-fed WTs and IP6K1-KOs. CD-KOs display higher VO_2 consumption following cold and cold + fast exposures (Figure 1D—F; 5 °C and 5 °C + fast). Activities are unchanged (Figure S1C). Carbohydrate-VO_2 is favored in cold-exposed CD-KOs, whereas fat-VO_2 is largely similar in both genotypes (Figure 1G and H). Enhanced EE protects CD-KOs from cold + fast induced decline in body temperature (Figure 1I). Mild hypothermia is observed under cold + fast conditions (Figure 1I), as only cold-exposed mice do not show the phenotype (Figure S1D). Together, these results indicate that although CD-fed IP6K1-KO mice do not display a noticeable increase in EE under basal conditions, they exhibit higher carbohydrate oxidation mediated EE under fasted/refed and cold-exposed conditions, which reduces energy accumulation.

3.2. Global IP6K1 deletion stimulates adipose tissue browning

Next, we determined whether enhanced thermogenic EE in the CD-KOs, is due to an increase in adipose tissue browning. Indeed, IWAT of CD-KOs appear smaller and brownish at 23 °C (Figure 2A). UCP1 and PGC1α protein levels are higher in IWAT and RWAT of CD-KOs (Figure 2B and C). We do not observe any alteration of these proteins in the BAT of CD-KOs (Figure S2A). Other browning and mitochondrial activity markers are also elevated in the RWAT and IWAT of CD-KOs (Figure 2D and E). Moreover, mitochondrial oxygen consumption rate (OCR) was increased in the CD-KO RWAT explants (Figure 2F). IP6K1 deletion enhanced OCR in beige adipocytes in vitro (Figure 2G and H and Figure S2B). Extracellular acidification rate (ECAR), which indirectly measures glycolytic rate, was similar in WT and IP6K1-KO beige adipocytes (Figure S2C). Thus, IP6K1 deletion enhanced adipose tissue browning mediated thermogenic EE.

3.3. HFD-fed IP6K1-KO mice exhibit higher fat oxidation at 23 °C, albeit switch to carbohydrate oxidation at 5 °C

Energy intake was similar in HFD-fed WTs and IP6K1-KOs (Table S2). However, HFD-KO mice displayed higher VO_2 and EE at both 23 °C and following cold and cold + fast exposures (Figure 3A—C). Activities were unaltered under these conditions (Figure S3A). At 23 °C, HFD-KO mice exhibited more fat-VO_2, albeit at 5 °C, they switched to carbohydrate-VO_2 (Figure 3D and E). Efficient carbohydrate EE protected HFD-KOs from acute cold + fast induced decline in body temperature (Figure 3F). HFD-KO mice also displayed higher UCP1 protein level in RWAT and IWAT depots (Figure 3G, Figure S3B). Moreover, they exhibited reduced adipocyte size and fat accumulation in various adipose tissue depots (Figure S3C—E). These results suggest that HFD-fed IP6K1-KOs exhibit enhanced fat oxidation at ambient temperature, albeit switch to carbohydrate oxidation following cold exposure. Moreover, efficient thermogenic EE protects these mice from HFD-induced weight gain.

3.4. Thermoneutrality delays, yet does not abolish the lean phenotype of HFD-fed IP6K1-KO mice

At 23 °C, global IP6K1-KOs were dramatically protected against HFD-induced weight gain [40]. The lean phenotype of IP6K1-KOs was evident from the onset of HFD-feeding [40] (Figure S4A). AdKO mice also displayed a similar phenotype [41], although the difference in weight gain between control and knockouts was more robust in the global knockouts [40,41]. Moreover, adipocyte-specific IP6K1 controls body weight primarily via regulation of adipose tissue browning mediated thermogenesis. Accordingly, the lean phenotype of HFD-fed AdKO mice was abolished at thermoneutral (30 °C) temperature [41]. Conversely, thermoneutrality impaired but does not abolish the lean phenotype of HFD-fed global IP6K1-KO mice (Figure S4B). Thus, after 4-weeks of HFD, IP6K1-KO mice, at 23 °C, gained ~7.6 g less body weight than WT (Figure S4A) whereas at 30 °C, they gained similar body weight (Figure S4B). After 4-weeks, IP6K1-KO mice exhibited a sluggish rate of weight gain (Figure S4B). At 23 °C, the difference in KO vs WT weight gain reached saturation by 6 weeks (Figure S4A), whereas at 30 °C, it took 14-weeks for the knockouts to attain such a difference (Figure S4B). After 14-weeks of HFD-feeding at 30 °C, HFD-KOs accumulated less total and percent (over total body weight) fat (Figure 4A and B). Total lean mass was lower, whereas percent lean mass was higher in the knockouts (Figure 4A and B). The knockouts accumulated less fat in various adipose-depots (Figure 4C and D). Moreover, the thermoneutral-KO mice were protected from fatty liver (Figure 4C and D). The knockouts also displayed reduced serum levels of triglycerides (TAG), cholesterol, HDL, and LDL (Figure 4E—H).

At 23 °C, HFD-KOs displayed lower blood glucose level than WT, after 8-weeks of HFD [40], whereas they were largely similar in both genotypes at 30 °C (Figure S4C; 8 wks). Similarly, after 8-weeks of HFD at 30 °C, the knockouts displayed a slight improvement in GTT (Figure S4D and E) compared to a substantial improvement at 23 °C [40]. After 14-weeks, blood glucose level was significantly higher, whereas glucose disposal (GTT) rate was lower, compared to knockouts (Figure 4I and J and Figure S4C; 14 wks). Accordingly, stimulatory phosphorylation of the insulin effector protein kinase Akt was higher in HFD-KO RWAT and liver (Figure 4K). Moreover, expression level of the insulin sensitizing adipokine adiponectin (AdipoQ) was significantly higher in the knockouts (Figure S4F). Monomeric AdipoQ generates low and high molecular weight oligomers (LMW and HMW), of which

Figure 6: IP6K1 enhances cellular fat accumulation by diminishing AMPK mediated energy metabolism. **A**. IP6K1-KO MEFs accumulate less fat following oleate (OA, 24 h) treatment. **B**. β (OA)-oxidation is increased in IP6K1-KO MEFs following OA (24 h) treatment. However, β (PA)-oxidation is increased under basal and PA (24 h) treated conditions (*n = 3; t-test*). **C**. AICAR treated IP6K1-KO MEFs display enhanced β-oxidation (*n = 3; two-way Anova*). **D**. Complementation of IP6K1-KO MEFs with active but not inactive Myc-IP6K1 restores OA-induced fat storage. **E**. Catalytically active but not inactive Myc-IP6K1 complementation reduces AICAR induced β-oxidation in IP6K1-KO MEFs (*n = 3; one-way Anova*). **F**. PGC1α mRNA expression is higher in IP6K1-KO MEFs, which is further enhanced by AICAR treatment (*n = 3; two-way Anova*). **G**. PGC1α protein level is higher in OA-treated IP6K1-KO MEFs. AMPK activity on PGC1α is also enhanced whereas PGC1α acetylation is reduced. **H**. AMPK stimulatory phosphorylation (T172) and its activity on ACC (S79) are enhanced in OA-treated IP6K1-KO MEFs. **I**. TNP enhances AMPK phosphorylation and activity in glucose starved 3T3L1 preadipocytes. Glucose induction reduces AMPK phosphorylation and activity in control but not in TNP treated cells. **J and K**. TNP enhances OCR in starved and glucose induced 3T3L1 preadipocytes (*8 replicates; t-test*). **L**. TNP enhances AMPK phosphorylation in 3T3L1 adipocytes, under basal conditions. AICAR was used as a positive control. **M**. TNP, at increasing concentrations, reduces fatty acid biosynthesis in 3T3L1 adipocytes. The ACC inhibitor TOFA was used as a positive control (*n = 3; one-way Anova*). **N**. CD-KOs, at 23 °C, display higher AMPK phosphorylation and activity in the RWAT depot. **O**. CD-KOs, at 23 °C, are sensitive to AICAR induced reduction in blood glucose level (*5—6 mice/group; two-way Anova*). In all panels, data are expressed as mean ± SEM. *P < 0.05, **P < 0.01, ***P < 0.001, ****P < 0.0001.

HMW is the potent insulin sensitizing form. Serum levels of HMW and LMW AdipoQ were significantly higher in the knockouts (Figure 4L and M and Figure S4G). Serum levels of total proteins were similar (Figure S4H). These results indicate that thermoneutrality delays, but does not abolish, manifestation of improved metabolic parameters in global IP6K1-KO mice.

3.5. HFD-fed IP6K1-KO mice display greater fat oxidation mediated EE at 30 °C

Next, we monitored adipose tissue browning and mitochondrial activity markers in thermoneutrally placed HFD-fed mice. Unlike HFD-fed AdKO, in which UCP1 is similarly expressed as LoxP control mice [41], global IP6K1-KO displayed a depot-specific UCP1 expression. For instance, RWAT-KO exhibited higher UCP1 mRNA and protein levels compared to RWAT-WT (Figure 5A and B; RWAT). Conversely, UCP1 mRNA levels were lower in the IWAT than RWAT and they are similar, whereas protein was undetectable in both genotypes (Figure 5A and B; IWAT). Similar to AdKO mice [41], we did not observe any alterations in tyrosine hydroxylase protein and pPKA substrate phosphorylation levels, indicating that sympathetic signaling is unaltered in global IP6K1-KO mice (data not shown). Plasma T3 levels were also similar in WT and IP6K1-KO mice at this condition, indicating that the hypothalamus—pituitary—thyroid axis is unaffected by IP6K1 deletion (Figure S5A). However, protein levels of DIO2 were augmented to a higher extent in the RWAT of IP6K1-KO mice, indicating that local alterations in thyroid signaling may alter UCP1 expression in the knockouts (Figure 5C and D and Figure S5B). On the other hand, expression levels of other mitochondrial energy oxidation markers were higher in both RWAT and IWAT depots of HFD-KOs at 30 °C, suggesting the possibility of UCP1 independent EE in the knockouts at thermoneutrality (Figure 5E and F).

Thereafter, we determined EE in thermoneutral HFD-fed mice. Thermoneutrally placed knockouts displayed higher VO_2 consumption and EE (Figure 5G and H and Figure S5C). Unlike cold exposed-KOs, thermoneutral-KOs exhibited a significant reduction in RER (Figure S5D). Consequently, thermoneutral-KOs oxidized more fat than WT (Figure 5I). Carbohydrate oxidation was slightly (not significant) less in the knockouts compared to WT, at this condition (Figure 5J). Total activity was similar in both genotypes (Figure S5E). Thus, global deletion of IP6K1 efficiently oxidized fat at thermoneutral conditions, presumably via UCP1 dependent and independent mechanisms, which protected the mice from DIO.

3.6. IP6K1 enhances cellular fat accumulation by diminishing AMPK mediated energy metabolism

The above studies demonstrate that IP6K1 deletion enhances efficient switching of carbohydrate and fat oxidation, depending on availability of the energy source. This unique quality protects IP6K1-KO mice from gaining body weight, even when they are exposed to a thermoneutral temperature. These results also indicate that, at least under thermoneutral conditions, HFD-KOs oxidize more fat via a mechanism that may or may not involve UCP1. Moreover, IP6K1 inhibits AMPK [41], which enhances global EE [20]. Therefore, we tested, whether IP6K1 regulates AMPK mediated energy metabolism in cells, which do not express UCP1. For this experiment, we simulated HFD-fed conditions in cells by treating them with the fatty acids oleate (OA) or palmitate (PA). We selected immortalized undifferentiated mouse embryonic fibroblast (MEF) cells for the study, as i) IP6K1 is the major 5-IP7 generating enzyme in these cells [44] and ii) they do not express UCP1. KO-MEFs accumulated 50% less fat (Figure 6A, Figure S6A). Less lipid accumulation was due to enhanced OA induced β-oxidation in IP6K1-KO MEFs (Figure 6B; OA). Similar results were obtained with PA, although its oxidation in the knockouts was enhanced even without PA-induction (24 h) (Figure 6B; PA). Fatty acid uptake was similar in both types (data not shown). Moreover, the β-oxidation stimulating action of the AMPK activator AICAR [25] was further enhanced in IP6K1-KO MEFs (Figure 6C). Expression of CPT1a was higher in KO-MEFs, which was further enhanced upon AICAR treatment (Figure S6B). Enhanced β-oxidation in the knockouts seems to be specific to AMPK pathway as pharmacologic modulators of sirtuins or other histone deacetylases (HDACs) did not modulate the process in the knockouts (Figure S6C). Complementation of IP6K1-KO MEFs with active, but not inactive, IP6K1 (Figure S6D) restored fat storing capacity of MEFs (Figure 6D). Moreover, active, but not inactive, IP6K1 complementation of IP6K1-KO MEFs reduced AICAR induced β-oxidation (Figure 6E). PGC1α mRNA levels, which were basally higher, were further elevated by AICAR (Figure 6F). PGC1α protein levels were also elevated in KO-MEFs upon OA treatment (Figure 6G). Moreover, PGC1α's acetylation (inhibitory modification) was decreased, while phosphorylation (stimulatory modification) was increased in OA-treated KO-MEFs (Figure 6G). AMPK stimulatory phosphorylation (T172) and its activity on ACC (S79) were also higher in OA-treated IP6K1-KO MEFs (Figure 6H).

Next, we tested IP6K1's effects on AMPK mediated energy metabolism in 3T3L1 cells. We used the IP6K inhibitor TNP for the following reasons; i) IP6K1 is the major isoform in the adipose tissue [39,41], ii) TNP significantly reduces 5-IP7 levels in 3T3L1 adipocytes [40], iii) TNP ameliorates DIO in mice by augmenting EE [43], and iv) TNP enhances AMPK signaling in the adipose tissue and adipocytes [41]. TNP protected glucose induction mediated inhibition of AMPK in 3T3L1 preadipocytes (Figure 6I). TNP enhanced OCR in starved and glucose-reintroduced 3T3L1 preadipocytes (Figure 6J and K). 3T3L1 preadipocytes did not express UCP1 and thus, the OCR was not due to uncoupling in these cells (Figure 6K). Maximal respiratory capacity of these cells was also enhanced by TNP (Figure 6K). Enhanced carbohydrate oxidation reduced fat accumulation in CD-KOs (Figure 1). It has been shown that AMPK inhibits fat generation from carbohydrates by inhibiting ACC mediated fatty acid biosynthesis [20]. We found that TNP enhanced AMPK activity in mature 3T3L1 adipocytes (Figure 6L) and inhibited fatty acid biosynthesis (Figure 6M). Similar to what happened in AdKO mice, AMPK stimulatory phosphorylation and its activity on ACC were substantially higher in the RWAT depot of CD-fed IP6K1-KO mice (Figure 6N). Hence, AICAR injection [49] significantly improved endogenous glucose disposal in CD-fed IP6K1-KO mice (Figure 6O). Thus, IP6K1 inhibited AMPK signaling, which reduced thermogenic [41] and non-thermogenic EE that promotes fat accumulation in vivo.

4. DISCUSSION

There are several major findings of the current study. One, global IP6K1 deletion protects mice from DIO and insulin resistance irrespective of environmental temperature conditions. Two, at 23 °C, CD-fed IP6K1-KO mice do not exhibit increased EE in ad libitum conditions, but they do so upon fasting and refeeding. Moreover, CD-fed knockouts expend more energy at 5 °C. In these conditions, CD-fed knockouts oxidize more carbohydrate, which answers the previously unsolved question, 'why do IP6K1-KO mice accumulate less fat, even in chow-fed conditions?' [40]. Three, HFD-fed IP6K1-KO mice oxidize more carbohydrate following cold exposure, whereas they oxidize

more fat at ambient and thermoneutral temperatures. Four, IP6K1-KO mice display enhanced UCP1 expression, which is partly impaired at 30 °C, although mitochondrial activity markers are higher in the knockouts irrespective of temperature conditions. Five, IP6K1 deletion enhances β-oxidation in a cell autonomous and UCP1 independent manner. Finally, IP6K1 regulates AMPK mediated fatty acid metabolism.

At 30 °C, HFD-KOs display higher UCP1 expression compared to WT, only in the RWAT, whereas expression of other mitochondrial biogenic/activity markers is elevated in both RWAT and IWAT of the knockouts. Functional differences including UCP1 expression among various WAT-depots, depending on diet and temperature conditions are reported [56], exert distinct effects on adipose tissue functions [4]. Proteomic studies of various WAT-depots also reveal substantial variations in their protein levels [57]. In male Wistar rats, UCP1 expression is higher in RWAT than IWAT under both CD and HFD-fed conditions, although other markers are expressed to comparable levels [58], which is in line with our observation. HFD-KOs display increased DIO2 primarily in the RWAT depot. DIO2 mediated T3 production enhances UCP1 expression. Accordingly, DIO2-KO mice display impaired UCP1 expression and thermogenesis [59]. Moreover, DIO2-KO mice are susceptible to DIO, fatty liver, and insulin resistance specifically at thermoneutral conditions, presumably due to a reduction in fat oxidation at this condition [60]. Thus, increased DIO2 levels may partly explain depot specific UCP1 expression, although further studies are needed to determine the precise mechanism. Involvement of one or more of other signaling pathways, such as FGF21, bile acids, and ANP/BNP, may also be involved in manifestation of the global IP6K1-KO mice phenotype. These possibilities will be tested in subsequent studies.

Our study also indicates that IP6K1 regulates AMPK mediated energy metabolism in UCP1 deficient cells. Similar to adipocytes, the AMPK-PGC1α axis is stimulated in IP6K1-KO MEFs. Under basal conditions, KO-MEFs display a higher ATP and NAD+/NADH ratio, due to enhanced glycolysis, as their mitochondrial respiratory capacity is partly compromised [61]. However, the β-oxidation machinery works more efficiently in KO-MEFs, especially when they are under excess energy (fatty acid) pressure. These results correlate with our in vivo observation that HFD-fed IP6K1-KO mice display more robust effects on EE and body weight compared to CD-fed knockouts. Future studies are needed to monitor effects of pharmacologic inhibition of IP6Ks on body weight and insulin sensitivity of UCP1-KO mice to precisely determine the extent to which IP6K1 regulates UCP1 independent EE in vivo.

In summary, deletion of global IP6K1 dramatically protects mice from DIO and insulin resistance due to increased EE, which is not entirely dependent on environmental temperature conditions. Pharmacologic inhibition of IP6Ks also produces similar results [43]. In general, clothing and other thermoregulatory conditions maintain the thermoneutral temperature in humans [62]. Therefore, a pathway that reduces body weight at thermoneutral temperature is a highly encouraging target in human obesity. AMPK mediated regulation of energy metabolism is well established in humans [18]. Moreover, deletion of IP6K3, which is the predominant isoform in murine and human skeletal muscle protects mice from age induced fat accumulation and insulin resistance. Moreover, IP6K3-KO mice live longer [39]. However, IP6K3-KO mice are not protected from DIO [39], which further suggests that IP6K1 regulates body weight primarily via its effects on the adipose tissue. Nevertheless, pan inhibition of the inositol pyrophosphate pathway is expected to have beneficial effects in obesity, diabetes, and aging.

FUNDING

This work is supported by DK1R01DK103746 and the TSRI startup fund 1-31564 to Anutosh Chakraborty.

AUTHOR CONTRIBUTIONS

A.C. conceived the project; A.C. and Q.Z. designed experiments; Q.Z. performed majority of the experiments; S.G. performed histology and immunohistochemistry; R.T. shared samples and reagents; A.C. and Q.Z. organized and analyzed data; A.C. wrote the manuscript. A.C. is the guarantor of this work and, as such, had full access to all the data in the study and takes responsibility for the integrity of the data and the accuracy of the data analysis.

COMPETING FINANCIAL INTERESTS

No competing financial interests.

ACKNOWLEDGEMENTS

We sincerely thank Prof. Solomon H. Snyder from the Johns Hopkins University School of Medicine for sharing IP6K1-KO mice, 3T3L1 preadipocytes, MEF, and other reagents. We thank Ted Kamenecka for providing critical inputs on the cellular β-oxidation assay, Andras Kern from Roy Smith's laboratory for sharing QPCR probes, Ana Rodrigues, Su Gao and Melissa Kazantzis for technical assistance, and the TSRI Metabolism and Aging department for sharing reagents and instruments.

CONFLICT OF INTEREST

None declared.

APPENDIX A. SUPPLEMENTARY DATA

Supplementary data related to this article can be found at http://dx.doi.org/10.1016/j.molmet.2016.11.010.

REFERENCES

[1] Harms, M., Seale, P., 2013. Brown and beige fat: development, function and therapeutic potential. Nature Medicine 19(10):1252–1263.
[2] Kozak, L.P., 2011. The genetics of brown adipocyte induction in white fat depots. Frontiers in Endocrinology (Lausanne) 2:64.
[3] Cinti, S., 2009. Transdifferentiation properties of adipocytes in the adipose organ. American Journal of Physiology. Endocrinology and Metabolism 297(5): E977–E986.
[4] Rosen, E.D., Spiegelman, B.M., 2014. What we talk about when we talk about fat. Cell 156(1–2):20–44.
[5] Nedergaard, J., Cannon, B., 2014. The browning of white adipose tissue: some burning issues. Cell Metabolism 20(3):396–407.
[6] Sidossis, L., Kajimura, S., 2015. Brown and beige fat in humans: thermogenic adipocytes that control energy and glucose homeostasis. Journal of Clinical Investigation 125(2):478–486.
[7] Whittle, A., Relat-Pardo, J., Vidal-Puig, A., 2013. Pharmacological strategies for targeting BAT thermogenesis. Trends in Pharmacological Sciences 34(6): 347–355.
[8] Collins, S., 2014. A heart-adipose tissue connection in the regulation of energy metabolism. Nature Reviews Endocrinology 10(3):157–163.
[9] Obregon, M.J., 2014. Adipose tissues and thyroid hormones. Frontiers in Physiology 5:479.

[10] Bianco, A.C., Kim, B.W., 2006. Deiodinases: implications of the local control of thyroid hormone action. Journal of Clinical Investigation 116(10): 2571–2579.
[11] Williams, G.R., Bassett, J.H., 2011. Deiodinases: the balance of thyroid hormone: local control of thyroid hormone action: role of type 2 deiodinase. Journal of Endocrinology 209(3):261–272.
[12] Arrojo, E.D.R., Fonseca, T.L., Werneck-de-Castro, J.P., Bianco, A.C., 2013. Role of the type 2 iodothyronine deiodinase (D2) in the control of thyroid hormone signaling. Biochimica et Biophysica Acta 1830(7):3956–3964.
[13] Kajimura, S., Spiegelman, B.M., Seale, P., 2015. Brown and beige fat: physiological roles beyond heat generation. Cell Metabolism 22(4):546–559.
[14] Granneman, J.G., Burnazi, M., Zhu, Z., Schwamb, L.A., 2003. White adipose tissue contributes to UCP1-independent thermogenesis. American Journal of Physiology. Endocrinology and Metabolism 285(6):E1230–E1236.
[15] Samms, R.J., Smith, D.P., Cheng, C.C., Antonellis, P.P., Perfield 2nd, J.W., Kharitonenkov, A., et al., 2015. Discrete aspects of FGF21 in vivo pharmacology do not require UCP1. Cell Reports 11(7):991–999.
[16] Veniant, M.M., Sivits, G., Helmering, J., Komorowski, R., Lee, J., Fan, W., et al., 2015. Pharmacologic effects of FGF21 are independent of the "browning" of white adipose tissue. Cell Metabolism 21(5):731–738.
[17] Finck, B.N., Kelly, D.P., 2006. PGC-1 coactivators: inducible regulators of energy metabolism in health and disease. Journal of Clinical Investigation 116(3):615–622.
[18] Steinberg, G.R., Kemp, B.E., 2009. AMPK in health and disease. Physiological Reviews 89(3):1025–1078.
[19] Mottillo, E.P., Desjardins, E.M., Crane, J.D., Smith, B.K., Green, A.E., Ducommun, S., et al., 2016. Lack of adipocyte AMPK exacerbates insulin resistance and hepatic steatosis through brown and beige adipose tissue function. Cell Metabolism 24(1):118–129.
[20] O'Neill, H.M., Holloway, G.P., Steinberg, G.R., 2013. AMPK regulation of fatty acid metabolism and mitochondrial biogenesis: implications for obesity. Molecular and Cellular Endocrinology 366(2):135–151.
[21] Zhang, H., Guan, M., Townsend, K.L., Huang, T.L., An, D., Yan, X., et al., 2015. MicroRNA-455 regulates brown adipogenesis via a novel HIF1an-AMPK-PGC1alpha signaling network. EMBO Reports 16(10):1378–1393.
[22] Canto, C., Gerhart-Hines, Z., Feige, J.N., Lagouge, M., Noriega, L., Milne, J.C., et al., 2009. AMPK regulates energy expenditure by modulating NAD+ metabolism and SIRT1 activity. Nature 458(7241):1056–1060.
[23] Zhang, Z., Zhang, H., Li, B., Meng, X., Wang, J., Zhang, Y., et al., 2014. Berberine activates thermogenesis in white and brown adipose tissue. Nature Communications 5:5493.
[24] Gaidhu, M.P., Frontini, A., Hung, S., Pistor, K., Cinti, S., Ceddia, R.B., 2011. Chronic AMP-kinase activation with AICAR reduces adiposity by remodeling adipocyte metabolism and increasing leptin sensitivity. The Journal of Lipid Research 52(9):1702–1711.
[25] Smith, A.C., Bruce, C.R., Dyck, D.J., 2005. AMP kinase activation with AICAR simultaneously increases fatty acid and glucose oxidation in resting rat soleus muscle. Journal of Physiology 565(Pt 2):537–546.
[26] Jager, S., Handschin, C., St-Pierre, J., Spiegelman, B.M., 2007. AMP-activated protein kinase (AMPK) action in skeletal muscle via direct phosphorylation of PGC-1alpha. Proceedings of the National Academy of Sciences of the United States of America 104(29):12017–12022.
[27] Wakil, S.J., Abu-Elheiga, L.A., 2009. Fatty acid metabolism: target for metabolic syndrome. The Journal of Lipid Research 50(Suppl):S138–S143.
[28] Wilson, M.S., Livermore, T.M., Saiardi, A., 2013. Inositol pyrophosphates: between signalling and metabolism. Biochemical Journal 452(3):369–379.
[29] Thota, S.G., Bhandari, R., 2015. The emerging roles of inositol pyrophosphates in eukaryotic cell physiology. Journal of Biosciences 40(3):593–605.
[30] Chakraborty, A., Kim, S., Snyder, S.H., 2011. Inositol pyrophosphates as mammalian cell signals. Science Signalling 4(188):re1.
[31] Barker, C.J., Illies, C., Gaboardi, G.C., Berggren, P.O., 2009. Inositol pyrophosphates: structure, enzymology and function. Cellular and Molecular Life Sciences 66(24):3851–3871.
[32] Thomas, M.P., Potter, B.V., 2014. The enzymes of human diphosphoinositol polyphosphate metabolism. The FEBS Journal 281(1):14–33.
[33] Wundenberg, T., Mayr, G.W., 2012. Synthesis and biological actions of diphosphoinositol phosphates (inositol pyrophosphates), regulators of cell homeostasis. Biological Chemistry 393(9):979–998.
[34] Shears, S.B., Baughman, B.M., Gu, C., Nair, V.S., Wang, H., 2016. The significance of the 1-kinase/1-phosphatase activities of the PPIP5K family. Advances in Biological Regulation.
[35] Wundenberg, T., Grabinski, N., Lin, H., Mayr, G.W., 2014. Discovery of InsP6-kinases as InsP6-dephosphorylating enzymes provides a new mechanism of cytosolic InsP6 degradation driven by the cellular ATP/ADP ratio. Biochemical Journal 462(1):173–184.
[36] Chakraborty, A., Latapy, C., Xu, J., Snyder, S.H., Beaulieu, J.M., 2014. Inositol hexakisphosphate kinase-1 regulates behavioral responses via GSK3 signaling pathways. Molecular Psychiatry 19(3):284–293.
[37] Ghoshal, S., Tyagi, R., Zhu, Q., Chakraborty, A., 2016. Inositol hexakisphosphate kinase-1 interacts with perilipin1 to modulate lipolysis. International Journal of Biochemistry & Cell Biology 78:149–155.
[38] Fu, C., Xu, J., Li, R.J., Crawford, J.A., Khan, A.B., Ma, T.M., et al., 2015. Inositol hexakisphosphate kinase-3 regulates the morphology and synapse formation of cerebellar purkinje cells via spectrin/adducin. Journal of Neuroscience 35(31):11056–11067.
[39] Moritoh, Y., Oka, M., Yasuhara, Y., Hozumi, H., Iwachidow, K., Fuse, H., et al., 2016. Inositol hexakisphosphate kinase 3 regulates metabolism and lifespan in mice. Scientific Reports 6:32072.
[40] Chakraborty, A., Koldobskiy, M.A., Bello, N.T., Maxwell, M., Potter, J.J., Juluri, K.R., et al., 2010. Inositol pyrophosphates inhibit Akt signaling, thereby regulating insulin sensitivity and weight gain. Cell 143(6):897–910.
[41] Zhu, Q., Ghoshal, S., Rodrigues, A., Gao, S., Asterian, A., Kamenecka, T.M., et al., 2016. Adipocyte-specific deletion of Ip6k1 reduces diet-induced obesity by enhancing AMPK-mediated thermogenesis. Journal of Clinical Investigation 126(11):4273–4288.
[42] Padmanabhan, U., Dollins, D.E., Fridy, P.C., York, J.D., Downes, C.P., 2009. Characterization of a selective inhibitor of inositol hexakisphosphate kinases: use in defining biological roles and metabolic relationships of inositol pyrophosphates. Journal of Biological Chemistry 284(16):10571–10582.
[43] Ghoshal, S., Zhu, Q., Asteian, A., Lin, H., Xu, H., Ernst, G., et al., 2016. TNP [N2-(m-Trifluorobenzyl), N6-(p-nitrobenzyl)purine] ameliorates diet induced obesity and insulin resistance via inhibition of the IP6K1 pathway. Molecular Metabolism 5(10):903–917.
[44] Bhandari, R., Juluri, K.R., Resnick, A.C., Snyder, S.H., 2008. Gene deletion of inositol hexakisphosphate kinase 1 reveals inositol pyrophosphate regulation of insulin secretion, growth, and spermiogenesis. Proceedings of the National Academy of Sciences of the United States of America 105(7):2349–2353.
[45] Petruzzelli, M., Schweiger, M., Schreiber, R., Campos-Olivas, R., Tsoli, M., Allen, J., et al., 2014. A switch from white to brown fat increases energy expenditure in cancer-associated cachexia. Cell Metabolism 20(3):433–447.
[46] Lusk, G., 1924. Animal calorimetry. Twenty-fourth paper. Analysis of the oxidation of mixtures of carbohydrate and fat. A correction. Journal of Biological Chemistry 59(1):41–42.
[47] Walden, T.B., Hansen, I.R., Timmons, J.A., Cannon, B., Nedergaard, J., 2012. Recruited vs. nonrecruited molecular signatures of brown, "brite," and white adipose tissues. American Journal of Physiology. Endocrinology and Metabolism 302(1):E19–E31.
[48] Mansuy-Aubert, V., Zhou, Q.L., Xie, X., Gong, Z., Huang, J.Y., Khan, A.R., et al., 2013. Imbalance between neutrophil elastase and its inhibitor alpha1-antitrypsin in obesity alters insulin sensitivity, inflammation, and energy expenditure. Cell Metabolism 17(4):534–548.

[49] Fujii, N., Hirshman, M.F., Kane, E.M., Ho, R.C., Peter, L.E., Seifert, M.M., et al., 2005. AMP-activated protein kinase alpha2 activity is not essential for contraction- and hyperosmolarity-induced glucose transport in skeletal muscle. Journal of Biological Chemistry 280(47):39033—39041.

[50] Gerhart-Hines, Z., Feng, D., Emmett, M.J., Everett, L.J., Loro, E., Briggs, E.R., et al., 2013. The nuclear receptor Rev-erbα controls circadian thermogenic plasticity. Nature 503:410—413.

[51] Brasaemle, D.L., Wolins, N.E., 2006. Isolation of lipid droplets from cells by density gradient centrifugation. Current Protocols in Cell Biology [Chapter 3]: p. Unit 3 15.

[52] Cousin, S.P., Hügl, S.R., Wrede, C.E., Kajio, H., Myers Jr., M.G., Rhodes, C.J., 2001. Free fatty acid-induced inhibition of glucose and insulin-like growth factor I-induced deoxyribonucleic acid synthesis in the pancreatic beta-cell line INS-1. Endocrinology 142(1):229—240.

[53] Rune, A., Osler, M.E., Fritz, T., Zierath, J.R., 2009. Regulation of skeletal muscle sucrose, non-fermenting 1/AMP-activated protein kinase-related kinase (SNARK) by metabolic stress and diabetes. Diabetologia 52(10):2182—2189.

[54] Kler, R.S., Sherratt, H.S., Turnbull, D.M., 1992. The measurement of mitochondrial beta-oxidation by release of 3H2O from [9,10-3H]hexadecanoate: application to skeletal muscle and the use of inhibitors as models of metabolic disease. Biochemical Medicine and Metabolic Biology 47(2):145—156.

[55] Landree, L.E., Hanlon, A.L., Strong, D.W., Rumbaugh, G., Miller, I.M., Thupari, J.N., et al., 2004. C75, a fatty acid synthase inhibitor, modulates AMP-activated protein kinase to alter neuronal energy metabolism. Journal of Biological Chemistry 279(5):3817—3827.

[56] Kozak, L.P., Anunciado-Koza, R., 2008. UCP1: its involvement and utility in obesity. International Journal of Obesity (London) 32(Suppl 7):S32—S38.

[57] Sackmann-Sala, L., Berryman, D.E., Munn, R.D., Lubbers, E.R., Kopchick, J.J., 2012. Heterogeneity among white adipose tissue depots in male C57BL/6J mice. Obesity (Silver Spring) 20(1):101—111.

[58] Garcia-Ruiz, E., Reynés, B., Díaz-Rúa, R., Ceresi, E., Oliver, P., Palou, A., 2015. The intake of high-fat diets induces the acquisition of brown adipocyte gene expression features in white adipose tissue. International Journal of Obesity (London) 39(11):1619—1629.

[59] Hall, J.A., Ribich, S., Christoffolete, M.A., Simovic, G., Correa-Medina, M., Patti, M.E., et al., 2010. Absence of thyroid hormone activation during development underlies a permanent defect in adaptive thermogenesis. Endocrinology 151(9):4573—4582.

[60] Castillo, M., Hall, J.A., Correa-Medina, M., Ueta, C., Kang, H.W., Cohen, D.E., et al., 2011. Disruption of thyroid hormone activation in type 2 deiodinase knockout mice causes obesity with glucose intolerance and liver steatosis only at thermoneutrality. Diabetes 60(4):1082—1089.

[61] Szijgyarto, Z., Garedew, A., Azevedo, C., Saiardi, A., 2011. Influence of inositol pyrophosphates on cellular energy dynamics. Science 334(6057):802—805.

[62] Tseng, Y.H., Cypess, A.M., Kahn, C.R., 2010. Cellular bioenergetics as a target for obesity therapy. Nature Reviews Drug Discovery 9(6):465—482.

